Simulation of the 3D Radiative Transfer with Anisotropic Scattering for Convective Trails

Olivier Pironneau, Pierre-Henri Tournier

Simulation of the 3D Radiative Transfer

with Anisotropic Scattering for Convective Trails

Olivier Pironneau and Pierre-Henri Tournier

Abstract

In two earlier publications we have proposed a numerical algorithm to solve the RTE in 3D based on an integro-differential formulation and iterations using $\mathcal{H}$-matrices to speed-up the computation of the integrals. In this article we show how the method can be extended to handle an important class of non-isotropic scattering for the atmosphere. An application to the Earth atmosphere is given.

1 Introduction

Airplane combustion engines generate $\mathtt{CO}_2$ (carbon dioxide), a gas which stays in the Earth atmosphere for ~ 500 years before being partially absorbed by the oceans.

Currently used fuels and potential future substitutes like hydrogen, synthetic or agricultural fuel combustion generate also $\mathtt{NO}_x$ (Nitrous oxides). Typically a nitrous oxide stays in the atmosphere ~ 100 years.

Carbon dioxide, nitrous oxides, methane, ozone and water vapor are "green house gases", (GHG), in the sense that atmospheric and past climates measurements indicate that they are most likely responsible for the additional heat received by Earth (global warming).

Olivier Pironneau
Applied Mathematics, Jacques-Louis Lions Lab, Sorbonne Université, 75252 Paris cedex 5, France, e-mail: olivier.pironneau@sorbonne-universite.fr

Pierre-Henri Tournier
Applied Mathematics, Jacques-Louis Lions Lab, Sorbonne Université, 75252 Paris cedex 5, France, e-mail: Pierre-Henri.Tournier@sorbonne-universite.fr

Air travel – around 100.000 flights/day – produces 3% of $\mathtt{CO}_2$ (or 12% of what is produced by all transport vehicles). It is still small, but the contribution of airplanes to global warming is expected to rise from today's $0.024W/m^2$ to $0.084W/m^2$ by 2050 [13].

A cloud similar to a cirrus, called "contrail (short for condensation trail) may appear in the airplane wake if atmospheric pressure and temperature are on the left side of a threshold curve, and further left of that pressure versus temperature curve the contrail will persist [14]. Several studies claim that these clouds have a warming effect perhaps 3 times stronger than the one caused by the combustion gases [12].

In the past few years the authors have worked to see if these claims could be validated by a numerical simulation of the fundamental equations of physics for these problems [2], [8], [9], [10]. we approach the problem from an applied mathematics point of view, with convergence error estimation and computational efficiency in mind.

The formation of a contrail has been simulated by solving the Navier-Stokes equations (NSE) with chemistry for the engine exhaust and phase change for the ice formation in the airplane wake (see [14]); it is the right approach to understand the mechanisms of the formation of contrails. Once the cloud is sufficiently developed one may study its effect on the absorption and scattering coefficients of the Radiative Transfer Equations (RTE) in the Earth atmosphere (see the data in [6]) and then solve the RTE-NSE system. The numerical simulations of RTE in one dimension is the object of intense research [5], [6], but mostly without coupling with a temperature equation or NSE.

In [7] and [15] we have proposed a numerical algorithm to solve the RTE in 3D based on an integro-differential formulation and iterations using $\mathcal{H}$-matrices to speed-up the computation of the integrals. In this article we show how the method can be extended to handle an important class of non-isotropic scattering for the atmosphere.

It is known that the preferred direction of scattering in clouds is the initial direction. It is modelled by an anisotropic probability of scattering (also called phase function) from $\boldsymbol{\omega}$ to $\boldsymbol{\omega}'$, $p_\nu(\boldsymbol{\omega}, \boldsymbol{\omega}')$ (see Figure 1).

2 The Radiative Transfer Equations

When molecular viscosity and wind convection are ignored, the temperature T in a medium exposed to electromagnetic waves satisfies the RTE as explained in [16]. It involves a frequency dependent radiation intensity field

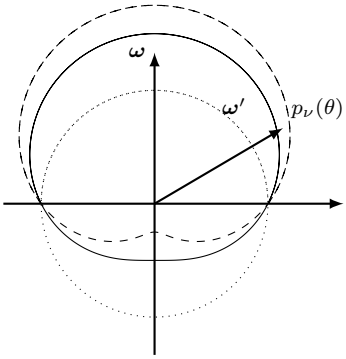

Fig. 1 This polar plot shows the probability $p(\theta)$ that a photon in the direction $\boldsymbol{\omega}$ scatters in the direction $\boldsymbol{\omega}' : p_\nu(\theta) = 1 + \frac{1}{2}\boldsymbol{\omega}\cdot\boldsymbol{\omega}' = 1 + \beta\cos(\theta)$ where θ is the angle $(\boldsymbol{\omega}, \boldsymbol{\omega}')$. The solid curve is for $\beta = \frac{1}{2}$, the dashed curve is for $\beta = 0.75$ and the dotted circle is the isotropic case is $\beta = 0$.

$I_\nu(\boldsymbol{x}, \boldsymbol{\omega})$ at position $\boldsymbol{x}$ in the physical domain Ω and in each direction $\boldsymbol{\omega}$. For all $\{\boldsymbol{x}, \boldsymbol{\omega}, \nu\} \in \Omega \times \mathbb{S}_2 \times \mathbb{R}^+$,

$$\begin{aligned} \boldsymbol{\omega}\cdot\boldsymbol{\nabla}_{\boldsymbol{x}} I_\nu + \rho\bar{\kappa}_\nu a_\nu \left[I_\nu - \frac{1}{4\pi}\int_{\mathbb{S}^2} p_\nu(\boldsymbol{\omega}, \boldsymbol{\omega}') I_\nu(\boldsymbol{\omega}')\mathrm{d}\omega' \right] \\ = \rho\bar{\kappa}_\nu(1 - a_\nu)[B_\nu(T) - I_\nu], \end{aligned} \tag{1}$$

$$\int_0^\infty \int_{\mathbb{S}^2} \rho\bar{\kappa}_\nu(1 - a_\nu)[B_\nu(T) - I_\nu]\mathrm{d}\omega\mathrm{d}\nu = 0,$$

where $\mathbb{S}^2$ is the unit sphere, $B_\nu(T) = \dfrac{2\hbar\nu^3}{c^2[\mathrm{e}^{\frac{\hbar\nu}{kT}} - 1]}$ is the Planck function, $\hbar, c, k$ are the Planck constant, the speed of light in the medium and the Boltzmann constant. The absorption coefficient $\kappa_\nu := \rho\bar{\kappa}_\nu$, where ρ is the medium density, comes from nuclear physics, but for our purpose it is seen as the percentage of radiation absorbed per unit length. The scattering albedo is $a_\nu \in (0, 1)$ and $p_\nu(\boldsymbol{\omega}, \boldsymbol{\omega}')$ is the probability that a ray in direction $\boldsymbol{\omega}$ scatters in direction $\boldsymbol{\omega}'$.

With appropriate boundary conditions, existence of solution has been established by [17] and [8]. In the latter, convergence of the following scheme was proved:

$$\begin{aligned} &\boldsymbol{\omega}\cdot\boldsymbol{\nabla} I_\nu^{n+1} + \kappa_\nu I_\nu^{n+1} = \frac{\kappa_\nu}{4\pi}\int_{\mathbb{S}^2} p_\nu(\boldsymbol{\omega}, \boldsymbol{\omega}') I_\nu^n(\boldsymbol{\omega}')d\omega' + \kappa_\nu(1 - a_\nu)B_\nu(T^n), \\ &\int_0^\infty \int_{\mathbb{S}^2} \kappa_\nu(1 - a_\nu)[B_\nu(T^{n+1}) - I_\nu^{n+1}]d\omega d\nu = 0. \end{aligned} \tag{2}$$

By the maximum principle for the first equation and the monotony of $T \mapsto B_\nu(T)$,

$$I^n \prec I^{n-1},\ \ T^n \prec T^{n-1} \quad \Longrightarrow \quad I^{n+1} \prec I^n, \qquad \Longrightarrow T^{n+1} \prec T^n,$$

where $a \prec b$ means $a(\boldsymbol{x}) \le b(\boldsymbol{x})$, for all $\boldsymbol{x}$ but not $a(\boldsymbol{x}) = b(\boldsymbol{x})$ everywhere. Hence by choosing $T^0 = 0$ and $I^0 = 0$, the positivity of T^1 and I^1 implies that $T^1 \prec T^0$, $I^1 \prec I^0$ so that , by induction, a strictly increasing sequence is obtained. Similarly a decreasing sequence is obtained if we manage $T^1 \succ T^0$, $I^1 \succ I^0$. As it was observed in [10] that the increasing sequences converge faster we will focus on that one only.

3 Integral Formulation

Consider an anisotropic scattering density

$$p_\nu(\boldsymbol{\omega}, \boldsymbol{\omega}') = 1 + \beta_\nu \boldsymbol{\omega} \cdot \boldsymbol{\omega}'.$$

Denote by Γ the boundary of Ω. One must find the radiation intensity $I_\nu(\boldsymbol{x}, \boldsymbol{\omega})$ at all points $\boldsymbol{x} \in \Omega$, for all directions all $\boldsymbol{\omega} \in \mathbb{S}^2$ and all radiation frequencies $\nu \in \mathbb{R}_+$, by solving the radiative transfer equations (RTE):

$$\boldsymbol{\omega} \cdot \nabla_x I_\nu + \kappa_\nu I_\nu = \kappa_\nu (1 - a_\nu) \left(B_\nu(T) + \beta_\nu \boldsymbol{\omega} \cdot \boldsymbol{K}_\nu \right) + \kappa_\nu a_\nu J_\nu \,, \tag{3}$$

$$J_\nu(\boldsymbol{x}) := \tfrac{1}{4\pi} \int_{\mathbb{S}^2} I_\nu \mathrm{d}\omega, \quad \boldsymbol{K}_\nu(\boldsymbol{x}) := \tfrac{1}{4\pi} \int_{\mathbb{S}^2} \boldsymbol{\omega} I_\nu(\boldsymbol{x}, \boldsymbol{\omega}) \mathrm{d}\omega \,, \tag{4}$$

$$\int_0^\infty \kappa_\nu (1 - a_\nu)(J_\nu - B_\nu(T)) \mathrm{d}\nu = 0 \,, \tag{5}$$

$$I_\nu(\boldsymbol{x}, \boldsymbol{\omega}) = R_\nu(\boldsymbol{x}, \boldsymbol{\omega}) I_\nu(\boldsymbol{x}, \boldsymbol{\omega} - 2(\boldsymbol{n} \cdot \boldsymbol{\omega})\boldsymbol{n}) + Q_\nu(\boldsymbol{x}, \boldsymbol{\omega}),$$
$$\text{on } \Sigma := \{ (\boldsymbol{x}, \boldsymbol{\omega}) \in \Gamma \times \mathbb{S}^2 \ : \ \boldsymbol{\omega} \cdot \boldsymbol{n}(\boldsymbol{x}) < 0 \}. \tag{6}$$

In (6), Q_ν is the radiation source and R_ν is the portion of radiation which is reflected by the boundary; $\boldsymbol{n}(\boldsymbol{x})$ is the outer normal of Γ at $\boldsymbol{x}$. $\kappa_\nu > 0$ and $a_\nu \in [0, 1]$ are the absorption and scattering coefficients; in general they depend on ν and $\boldsymbol{x}$.

The general solution of (3) is

$$I(\boldsymbol{x}, \boldsymbol{\omega}) = I(\boldsymbol{x}_\Sigma(\boldsymbol{x}, \boldsymbol{\omega}), \boldsymbol{\omega}) \mathrm{e}^{-\int_0^{\tau_{\boldsymbol{x},\boldsymbol{\omega}}} \kappa(\boldsymbol{x} - \boldsymbol{\omega} s) \mathrm{d}s} + \int_0^{\tau_{\boldsymbol{x},\boldsymbol{\omega}}} \mathrm{e}^{-\int_0^s \kappa(\boldsymbol{x} - \boldsymbol{\omega} s') \mathrm{d}s'} S_\nu(\boldsymbol{x} - \boldsymbol{\omega} s, \boldsymbol{\omega}) \mathrm{d}s,$$

where $\tau_{\boldsymbol{x},\boldsymbol{\omega}}$ is the length $|\boldsymbol{x} - \boldsymbol{x}_\Sigma(\boldsymbol{x}, \boldsymbol{\omega})|$, and $\mathcal{S}_\nu$ denotes its right-hand side,

$$\mathcal{S}_\nu(\boldsymbol{x}, \boldsymbol{\omega}) = \kappa_\nu(\boldsymbol{x})(1 - a_\nu(\boldsymbol{x})) \left(B_\nu(T(\boldsymbol{x})) + \beta_\nu(\boldsymbol{x}) \boldsymbol{\omega} \cdot \boldsymbol{K}_\nu(\boldsymbol{x}) \right) + \kappa_\nu(\boldsymbol{x}) a_\nu(\boldsymbol{x}) J_\nu(\boldsymbol{x}) \,. \tag{7}$$

3.1 Solution in Absence of Reflective Boundaries

Let us denote $\int_{[\boldsymbol{x},\boldsymbol{y}]} \kappa := \int_0^{|\boldsymbol{y}-\boldsymbol{x}|} \kappa(\boldsymbol{x}+s(\boldsymbol{y}-\boldsymbol{x}))\mathrm{d}s$. When $R_\nu = 0$, the following holds:

Proposition 1

$$J_\nu(\boldsymbol{x}) = S_\nu^E(\boldsymbol{x}) + \mathcal{J}[\mathcal{S}_\nu](\boldsymbol{x}), \tag{8}$$

$$S_\nu^E(\boldsymbol{x}) = \tfrac{1}{4\pi}\int_\Gamma Q_\nu(\boldsymbol{y}, \tfrac{\boldsymbol{y}-\boldsymbol{x}}{|\boldsymbol{y}-\boldsymbol{x}|})\frac{[(\boldsymbol{y}-\boldsymbol{x})\cdot\boldsymbol{n}(\boldsymbol{y})]_-}{|\boldsymbol{y}-\boldsymbol{x}|^3}\mathrm{e}^{-\int_{[\boldsymbol{x},\boldsymbol{y}]}\kappa}\mathrm{d}\Gamma(\boldsymbol{y}), \tag{9}$$

$$\mathcal{J}[\mathcal{S}_\nu](\boldsymbol{x}) = \tfrac{1}{4\pi}\int_\Omega \frac{\mathrm{e}^{-\int_{[\boldsymbol{x},\boldsymbol{y}]}\kappa}}{|\boldsymbol{y}-\boldsymbol{x}|^2}\mathcal{S}_\nu(\boldsymbol{y}, \frac{\boldsymbol{y}-\boldsymbol{x}}{|\boldsymbol{y}-\boldsymbol{x}|})\mathrm{d}\boldsymbol{y}. \tag{10}$$

Averaging (7) on $\mathbb{S}^2$ after multiplication by $\boldsymbol{\omega}$ leads to

$$\begin{aligned}
\boldsymbol{K}_\nu(\boldsymbol{x}) &:= \tfrac{1}{4\pi}\int_{\mathbb{S}^2}\boldsymbol{\omega} I(\boldsymbol{x},\boldsymbol{\omega})\mathrm{d}\omega = \boldsymbol{K}_\nu^E(\boldsymbol{x}) + \mathcal{K}[\mathcal{S}_\nu](\boldsymbol{x}) \quad \text{with}\\
\boldsymbol{K}_\nu^E(\boldsymbol{x}) &:= \tfrac{1}{4\pi}\int_{\mathbb{S}^2}\boldsymbol{\omega} I(\boldsymbol{x}_\Sigma(\boldsymbol{x},\boldsymbol{\omega}),\boldsymbol{\omega})\mathrm{e}^{-\int_0^{\tau_{\boldsymbol{x},\boldsymbol{\omega}}}\kappa(\boldsymbol{x}-\boldsymbol{\omega}s)\mathrm{d}s}\mathrm{d}\omega\\
&= \tfrac{1}{4\pi}\int_\Gamma(\boldsymbol{y}-\boldsymbol{x})Q_\nu(\boldsymbol{y}, \tfrac{\boldsymbol{y}-\boldsymbol{x}}{|\boldsymbol{y}-\boldsymbol{x}|})\frac{[(\boldsymbol{y}-\boldsymbol{x})\cdot\boldsymbol{n}(\boldsymbol{y})]_-}{|\boldsymbol{y}-\boldsymbol{x}|^4}\mathrm{e}^{-\int_{[\boldsymbol{x},\boldsymbol{y}]}\kappa}\mathrm{d}\Gamma(\boldsymbol{y}),\\
\mathcal{K}[\mathcal{S}_\nu](\boldsymbol{x}) &:= \tfrac{1}{4\pi}\int_{\mathbb{S}^2}\int_0^{\tau_{\boldsymbol{x},\boldsymbol{\omega}}}\boldsymbol{\omega}\mathrm{e}^{-\int_0^s\kappa(\boldsymbol{x}-\boldsymbol{\omega}s')\mathrm{d}s'}\mathcal{S}_\nu(\boldsymbol{x}-\boldsymbol{\omega}s,\boldsymbol{\omega})\mathrm{d}s\mathrm{d}\omega\\
&= \tfrac{1}{4\pi}\int_\Omega(\boldsymbol{y}-\boldsymbol{x})\mathcal{S}_\nu(\boldsymbol{y}, \tfrac{\boldsymbol{y}-\boldsymbol{x}}{|\boldsymbol{y}-\boldsymbol{x}|})\frac{\mathrm{e}^{-\int_{[\boldsymbol{x},\boldsymbol{y}]}\kappa}}{|\boldsymbol{y}-\boldsymbol{x}|^3}\mathrm{d}\boldsymbol{y}.
\end{aligned} \tag{11}$$

3.2 Iterative Method

In [7] it was shown that, in absence of $\boldsymbol{K}_\nu$, i.e. $\beta_\nu = 0$, the following is monotone and convergent. Its extension to $\beta_\nu > 0$ is:

Algorithm

1. Initialize J_ν, $\boldsymbol{K}_\nu$ and T (by zero, for instance).
2. Compute $\mathcal{S}_\nu$ by (7).
3. Update J_ν by (11),(9), (10) and $\boldsymbol{K}_\nu$ by (11).
4. Update T by solving (5).

4 Extension to Reflective Conditions (RC)

As in [15], consider boundary condition (6). Proposition 1 can be extended to case with RC and in the case of non-multiple reflection, it becomes:

Proposition 2 *The same iterations are proposed with*

$$J_\nu(\boldsymbol{x}) = S^E_{\nu,1}(\boldsymbol{x})+S^E_{\nu,2}(\boldsymbol{x})+\bar{\mathcal{J}}[\mathcal{S}_\nu](\boldsymbol{x}), \quad \boldsymbol{K}_\nu(\boldsymbol{x}) = \boldsymbol{K}^E_{\nu,1}(\boldsymbol{x})+\boldsymbol{K}^E_{\nu,2}(\boldsymbol{x})+\bar{\mathcal{K}}[\mathcal{S}_\nu](\boldsymbol{x}), \tag{12}$$

$$S^E_{\nu,1}(\boldsymbol{x}) = \tfrac{1}{4\pi}\int_\Gamma Q_\nu(\boldsymbol{y}, \tfrac{\boldsymbol{y}-\boldsymbol{x}}{|\boldsymbol{y}-\boldsymbol{x}|})\frac{[(\boldsymbol{y}-\boldsymbol{x})\cdot\boldsymbol{n}(\boldsymbol{y})]_-}{|\boldsymbol{y}-\boldsymbol{x}|^3}\mathrm{e}^{-\int_{[\boldsymbol{x},\boldsymbol{y}]}\kappa}\mathrm{d}\Gamma(\boldsymbol{y}),$$

$$S^E_{\nu,2}(\boldsymbol{x}) = \sum_{n=1}^M \tfrac{1}{4\pi}\int_\Gamma R_\nu(\boldsymbol{x}'_n, \tfrac{\boldsymbol{x}-\boldsymbol{x}'_n}{|\boldsymbol{x}-\boldsymbol{x}'_n|})Q_\nu(\boldsymbol{y}, \tfrac{\boldsymbol{x}'_n-\boldsymbol{y}}{|\boldsymbol{x}'_n-\boldsymbol{y}|})$$
$$\times \frac{[(\boldsymbol{x}'_n-\boldsymbol{y})\cdot\boldsymbol{n}(\boldsymbol{y})]_-\mathrm{e}^{-\int_{[\boldsymbol{x},\boldsymbol{x}'_n]\cup[\boldsymbol{x}'_n,\boldsymbol{y}]}\kappa}}{|\boldsymbol{x}'_n-\boldsymbol{y}|\,(|\boldsymbol{x}-\boldsymbol{x}'_n|+|\boldsymbol{x}'_n-\boldsymbol{y}|)^2}\mathrm{d}\Gamma(\boldsymbol{y}).$$

$$\bar{\mathcal{J}}[\mathcal{S}_\nu](\boldsymbol{x}) = \tfrac{1}{4\pi}\int_\Omega\left[\frac{\mathrm{e}^{-\int_{[\boldsymbol{x},\boldsymbol{y}]}\kappa}}{|\boldsymbol{y}-\boldsymbol{x}|^2}\right.$$
$$\left.+\sum_{n=1}^M \frac{\mathrm{e}^{-\int_{[\boldsymbol{x},\boldsymbol{x}'_n]\cup[\boldsymbol{x}'_n,\boldsymbol{y}]}\kappa}}{(|\boldsymbol{x}-\boldsymbol{x}'_n|+|\boldsymbol{x}'_n-\boldsymbol{y}|)^2}R_\nu(\boldsymbol{x}'_n, \tfrac{\boldsymbol{x}-\boldsymbol{x}'_n}{|\boldsymbol{x}-\boldsymbol{x}'_n|})\right]\mathcal{S}_\nu(\boldsymbol{y}, \tfrac{\boldsymbol{y}-\boldsymbol{x}}{|\boldsymbol{y}-\boldsymbol{x}|})\mathrm{d}\boldsymbol{y}. \tag{13}$$

$$\boldsymbol{K}^E_{\nu,1}(\boldsymbol{x}) = \tfrac{1}{4\pi}\int_\Gamma (\boldsymbol{y}-\boldsymbol{x})Q_\nu(\boldsymbol{y}, \tfrac{\boldsymbol{y}-\boldsymbol{x}}{|\boldsymbol{y}-\boldsymbol{x}|})\frac{[(\boldsymbol{y}-\boldsymbol{x})\cdot\boldsymbol{n}(\boldsymbol{y})]_-}{|\boldsymbol{y}-\boldsymbol{x}|^3}\mathrm{e}^{-\int_{[\boldsymbol{x},\boldsymbol{y}]}\kappa}\mathrm{d}\Gamma(\boldsymbol{y}),$$

$$\boldsymbol{K}^E_{\nu,2}(\boldsymbol{x}) = \sum_{n=1}^M \tfrac{1}{4\pi}\int_\Gamma (\boldsymbol{x}-\boldsymbol{x}'_n)R_\nu(\boldsymbol{x}'_n, \tfrac{\boldsymbol{x}-\boldsymbol{x}'_n}{|\boldsymbol{x}-\boldsymbol{x}'_n|})Q_\nu(\boldsymbol{y}, \tfrac{\boldsymbol{x}'_n-\boldsymbol{y}}{|\boldsymbol{x}'_n-\boldsymbol{y}|})$$
$$\times \frac{[(\boldsymbol{x}'_n-\boldsymbol{y})\cdot\boldsymbol{n}(\boldsymbol{y})]_-\mathrm{e}^{-\int_{[\boldsymbol{x},\boldsymbol{x}'_n]\cup[\boldsymbol{x}'_n,\boldsymbol{y}]}\kappa}}{|\boldsymbol{x}'_n-\boldsymbol{y}|\,(|\boldsymbol{x}-\boldsymbol{x}'_n|+|\boldsymbol{x}'_n-\boldsymbol{y}|)^2}\mathrm{d}\Gamma(\boldsymbol{y}),$$

$$\bar{\mathcal{K}}[\mathcal{S}_\nu](\boldsymbol{x}) = \tfrac{1}{4\pi}\int_\Omega\left[\frac{\boldsymbol{y}-\boldsymbol{x}}{|\boldsymbol{y}-\boldsymbol{x}|^3}\mathrm{e}^{-\int_{[\boldsymbol{x},\boldsymbol{y}]}\kappa}\right.$$
$$\left.+\sum_{n=1}^M (\boldsymbol{x}-\boldsymbol{x}'_n)\frac{\mathrm{e}^{-\int_{[\boldsymbol{x},\boldsymbol{x}'_n]\cup[\boldsymbol{x}'_n,\boldsymbol{y}]}\kappa}}{(|\boldsymbol{x}-\boldsymbol{x}'_n|+|\boldsymbol{x}'_n-\boldsymbol{y}|)^2}R_\nu(\boldsymbol{x}'_n, \tfrac{\boldsymbol{x}-\boldsymbol{x}'_n}{|\boldsymbol{x}-\boldsymbol{x}'_n|})\right]\mathcal{S}_\nu(\boldsymbol{y}, \tfrac{\boldsymbol{y}-\boldsymbol{x}}{|\boldsymbol{y}-\boldsymbol{x}|})\mathrm{d}\boldsymbol{y}. \tag{14}$$

where M is the number of RC boundaries and $\boldsymbol{x}'_n$ is the point of reflection on the boundary of the ray going from $\boldsymbol{x}$ to $\boldsymbol{y}$ via $\boldsymbol{x}'_n$.

All equations are discretized using a P^1 finite element framework. Some integrals have a singular kernel, so a careful quadrature should be used.

In [7], [15] a strategy is explained to compute all the integrals as a matrix vector product where the matrices are hierarchical compressed $\mathcal{H}$-matrices [3],[4],[11].

In the grey case (κ_ν independent of ν) we need 5+M matrices. This could be taxing in computer memory, but not in computing time because the core of the method is $N \ln N$ where N is the number of finite element vertices.

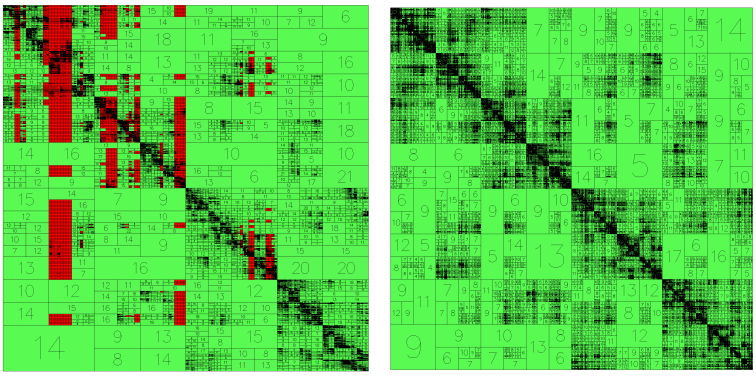

Fig. 2 Visual representations of the $\mathcal{H}$-matrices surface-to-volume on the left and volume-to-volume on the right, for the computation of the temperature in the Chamonix valley. The level of compression is shown by light green-to-red and the numbers correspond to the rank of the truncated SVD approximation of each block.

In the non grey case we need P(5+M) matrices where P is the number of values taken by the numerical approximation of κ_ν.

5 The Stratified One Dimensional Approximation

Let us consider the Earth's atmosphere submitted to black body radiations from the sun at temperature T_S and earth at T_E. The atmosphere is thin and the Sun is far. As a first approximation the ground is locally flat and has a negligible relief. Then all quantities are only function of the altitude z and independent of x and y. This, so called, stratified approximation of the RTE is (see [2])

$$(\mu\partial_\tau + \kappa_\nu) I_\nu(\tau,\mu) = \kappa_\nu(1-a_\nu)B_\nu(T(\tau)) + \tfrac{1}{2}\kappa_\nu a_\nu \int_{-1}^{1} p_\nu(\mu,\mu') I_\nu(\tau,\mu')\mathrm{d}\mu' \,, \tag{15}$$

$$I_\nu(0,\mu) = r_\nu I(0,-\mu) + \mu Q_\nu^+ \,, \quad I_\nu(Z,-\mu) = \mu Q_\nu^- \,, \qquad 0<\mu<1 \,, \tag{16}$$

$$\int_0^\infty \kappa_\nu(1-a_\nu)B_\nu(T(\tau))\mathrm{d}\nu = \int_0^\infty \kappa_\nu(1-a_\nu)J_\nu(\tau)\mathrm{d}\nu, \tag{17}$$

with

$$Q_\nu^+ = Q^E B_\nu(T_E), \quad Q_\nu^- = Q^S B_\nu(T_S), \quad J_\nu(\tau) := \tfrac{1}{2}\int_{-1}^{1} I_\nu(\tau,\mu)\mathrm{d}\mu, \tag{18}$$

where μ is the cosine of $\boldsymbol{\omega}$ with the vertical direction and τ is the optical thickness:

$$\tau = \int_0^z \rho(z')\mathrm{d}z'.$$

5.1 RTE with Non-Isotropic and Rayleigh Phase Function

The scattering function is $p_\nu(\mu,\mu') = 1 + \beta_\nu\mu'$ in a cloud between altitude Z_m and Z_M and at high altitude $z > Z_M$ it is the Rayleigh phase function $p_\nu(\mu,\mu') = \frac{3}{16}(3-\mu^2) + \frac{3}{16}(3\mu^2-1)\mu'^2$. It is combined into one formula with two given altitudes and possibly frequency dependent functions $b_\nu(\tau)$ and $\beta_\nu(\tau)$ in $[0,1]$,

$$p_\nu(\mu,\mu') = b_\nu + \beta_\nu\mu' + \tfrac{3}{16}(1-b_\nu)(3-\mu^2+(3\mu^2-1)\mu'^2). \tag{19}$$

Observe that $p_\nu(\mu,\mu') \geq 0$ and $\frac{1}{2}\int_{-1}^{1} p_\nu(\mu,\mu')\mathrm{d}\mu' = 1$. Keeping (17) as the defining equation for T, given I, the problem becomes

$$\begin{cases} (\mu\partial_\tau + \kappa_\nu)I_\nu(\tau,\mu) = \mathcal{S}_\nu(\tau) := \mathcal{R}_\nu(\tau) + \mathcal{P}_\nu(\tau)\mu^2\,, \\ I_\nu(0,\mu) = r_\nu I(0,-\mu) + \mu Q_\nu^+\,, \quad I_\nu(Z,-\mu) = \mu Q_\nu^-\,, \qquad 0<\mu<1\,, \end{cases} \tag{20}$$

with

$$\begin{aligned} K_\nu(\tau) :=& \tfrac{1}{2}\int_{-1}^{1} \mu I_\nu(\tau,\mu)\mathrm{d}\mu\,, \qquad L_\nu(\tau) = \tfrac{1}{2}\int_{-1}^{1}\mu^2 I_\nu \mathrm{d}\mu\,, \\ \mathcal{R}_\nu(\tau) :=& \kappa_\nu a_\nu\left((\tfrac{7}{16}b + \tfrac{9}{16})J_\nu(\tau) + \beta K_\nu(\tau) - \tfrac{3}{16}(1-b)L_\nu(\tau)\right) + \kappa_\nu(1-a_\nu)B_\nu(T(\tau))\,, \\ \mathcal{P}_\nu(\tau) :=& \tfrac{3}{16}(1-b)(-J_\nu(\tau) + 3L_\nu(\tau)) \end{aligned} \tag{21}$$

and (17).

Algorithm

1. Initialize $J_\nu^0(\tau,\mu) = 0$, $K_\nu^0(\tau,\mu) = 0$, $L_\nu^0(\tau,\mu) = 0$ and $T^0(\tau) = 0$.
2. Compute I^{n+1} by (20) with $\mathcal{S}_\nu^n$.
3. Update $J_\nu^{n+1}(\tau,\mu)$, $K_\nu^{n+1}(\tau,\mu)$, $L_\nu^{n+1}(\tau,\mu)$ by (21), then $\mathcal{R}_\nu(\tau)$ and $\mathcal{P}_\nu(\tau)$.
4. Then, compute T^{n+1} by solving (17).

5.2 Implementation

Recall the definition of the exponential integrals

$$E_p(X) := \int_0^1 e^{-X/\mu}\mu^{p-2}\mathrm{d}\mu\,, \qquad X > 0\,. \tag{22}$$

For $i = 3, 4, 5$, let

$$\begin{aligned} S_i(\nu,\tau) &:= \tfrac{1}{2}E_i(\kappa_\nu\tau)Q^+(\tau) + \tfrac{(-1)^{i-1}}{2}(E_i(\kappa_\nu(Z-\tau)) + r_\nu E_i(\kappa_\nu(Z+\tau)))Q^-(\tau),\\ F_i(\tau,t) &:= \tfrac{1}{2}E_3(\kappa_\nu|\tau-t|) + \tfrac{r_\nu}{2}E_3(\kappa_\nu|\tau+t|). \end{aligned} \tag{23}$$

Proposition 3 *With* (21) *and* (23) *the quantities needed by the algorithm above are given by*

$$\begin{aligned} J_\nu^{n+1}(\tau) =& S_3(\nu,\tau) + \tfrac{1}{2}\int_0^Z F_1(\tau,t)\mathcal{R}_\nu^n(\tau)\mathrm{d}t + \tfrac{1}{2}\int_0^Z F_3(\tau,t)\mathcal{P}_\nu^n(\tau)\mathrm{d}t\,,\\ K_\nu^{n+1}(\tau) =& S_4(\nu,\tau) + \tfrac{1}{2}\int_0^\tau F_2(\tau,t)\mathcal{R}_\nu^n(t)\mathrm{d}t + \tfrac{1}{2}\int_0^\tau F_4(\tau,t)\mathcal{P}_\nu^n(t)\mathrm{d}t\\ &- \tfrac{1}{2}\int_\tau^Z F_2(\tau,t)\mathcal{R}_\nu^n(t)\mathrm{d}t - \tfrac{1}{2}\int_\tau^Z F_4(\tau,t)\mathcal{P}_\nu^n(t)\mathrm{d}t\,,\\ L_\nu^{n+1}(\tau) =& S_5(\nu,\tau) + \tfrac{1}{2}\int_0^Z F_3(\tau,t)\mathcal{R}_\nu^n(\tau)\mathrm{d}t + \tfrac{1}{2}\int_0^Z F_5(\tau,t)\mathcal{P}_\nu^n(\tau)\mathrm{d}t\,. \end{aligned} \tag{24}$$

Proof For clarity let us assume that $r_\nu = 0$. For the general case see [9]. Applying the method of characteristics shows that

$$\begin{aligned} I_\nu(\tau,\mu) &= \mu e^{-\frac{\kappa_\nu\tau}{\mu}}Q_\nu^+\mathbf{1}_{\mu>0} + |\mu|e^{-\frac{\kappa_\nu(Z-\tau)}{|\mu|}}Q_\nu^-\mathbf{1}_{\mu<0}\\ &\quad + \mathbf{1}_{\mu>0}\int_0^\tau e^{-\frac{\kappa_\nu(\tau-t)}{\mu}}\frac{\kappa_\nu}{\mu}\mathcal{S}_\nu(t)\mathrm{d}t + \mathbf{1}_{\mu<0}\int_\tau^Z e^{-\frac{\kappa_\nu(t-\tau)}{|\mu|}}\frac{\kappa_\nu}{|\mu|}\mathcal{S}_\nu(t)\mathrm{d}t\,. \end{aligned} \tag{25}$$

Therefore with $k = 0$ or $k = 2$,

$$
\begin{aligned}
&\int_{-1}^{1}\mu^k I_\nu(\tau,\mu)\mathrm{d}\mu = \int_{-1}^{1}|\mu|^{k+1}\Big(e^{-\frac{\kappa_\nu\tau}{\mu}}Q_\nu^+\mathbf{1}_{\mu>0}+e^{-\frac{\kappa_\nu(Z-\tau)}{|\mu|}}Q_\nu^-\mathbf{1}_{\mu<0}\Big)\mathrm{d}\mu\\
&+\int_{-1}^{1}|\mu|^{k-1}\Big(\mathbf{1}_{\mu>0}\int_0^\tau e^{-\frac{\kappa_\nu(\tau-t)}{\mu}}\kappa_\nu\mathcal{S}_\nu(t)\mathrm{d}t+\mathbf{1}_{\mu<0}\int_\tau^Z e^{-\frac{\kappa_\nu(t-\tau)}{|\mu|}}\kappa_\nu\mathcal{S}_\nu(t)\mathrm{d}t\Big)\mathrm{d}\mu\\
&=\int_0^1|\mu|^{k+1}e^{-\frac{\kappa_\nu\tau}{\mu}}Q_\nu^+\mathrm{d}\mu+\int_{-1}^0|\mu|^{k+1}e^{-\frac{\kappa_\nu(Z-\tau)}{|\mu|}}Q_\nu^-\mathrm{d}\mu\\
&+\int_0^1|\mu|^{k-1}\int_0^\tau e^{-\frac{\kappa_\nu(\tau-t)}{\mu}}\kappa_\nu\mathcal{S}_\nu(t)\mathrm{d}t+\int_{-1}^0|\mu|^{k-1}\int_\tau^Z e^{-\frac{\kappa_\nu(t-\tau)}{|\mu|}}\kappa_\nu\mathcal{S}_\nu(t)\mathrm{d}t\mathrm{d}\mu\\
&=\int_0^1|\mu|^{k+1}\left(e^{-\frac{\kappa_\nu\tau}{\mu}}Q_\nu^+ + e^{-\frac{\kappa_\nu(Z-\tau)}{|\mu|}}Q_\nu^-\right)\mathrm{d}\mu\\
&+\int_0^\tau\int_0^1|\mu|^{k-1}e^{-\frac{\kappa_\nu(\tau-t)}{\mu}}\kappa_\nu(\mathcal{R}_\nu(t)+\mathcal{P}_\nu(t)\mu^2)\mathrm{d}\mu\mathrm{d}t\\
&+\int_\tau^Z\int_0^1|\mu|^{k-1}e^{-\frac{\kappa_\nu(t-\tau)}{|\mu|}}\kappa_\nu(\mathcal{R}_\nu(t)+\mathcal{P}_\nu(t)\mu^2)\mathrm{d}\mu\mathrm{d}t\\
&=E_{k+3}(\kappa_\nu\tau)Q_\nu^+ + E_{k+3}(\kappa_\nu(Z-\tau))Q^-\\
&+\int_0^\tau E_{k+1}(\kappa_\nu(\tau-t))R_\nu(t)\mathrm{d}t+\int_\tau^Z E_{k+1}(\kappa_\nu(t-\tau))R_\nu(t)\mathrm{d}t\\
&+\int_0^\tau E_{k+3}(\kappa_\nu(\tau-t))P_\nu(t)\mathrm{d}t+\int_\tau^Z E_{k+3}(\kappa_\nu(t-\tau))P_\nu(t)\mathrm{d}t.
\end{aligned}
\tag{26}
$$

For $k=1$, the same computation gives

$$
\begin{aligned}
&\int_{-1}^{1}\mu I_\nu(\tau,\mu)\mathrm{d}\mu = \int_{-1}^{1}\mu^2\Big(e^{-\frac{\kappa_\nu\tau}{\mu}}Q_\nu^+\mathbf{1}_{\mu>0}-e^{-\frac{\kappa_\nu(Z-\tau)}{|\mu|}}Q_\nu^-\mathbf{1}_{\mu<0}\Big)\mathrm{d}\mu\\
&+\int_{-1}^{1}\Big(\mathbf{1}_{\mu>0}\int_0^\tau e^{-\frac{\kappa_\nu(\tau-t)}{\mu}}\kappa_\nu\mathcal{S}_\nu(t)\mathrm{d}t-\mathbf{1}_{\mu<0}\int_\tau^Z e^{-\frac{\kappa_\nu(t-\tau)}{|\mu|}}\kappa_\nu\mathcal{S}_\nu(t)\mathrm{d}t\Big)\mathrm{d}\mu\\
&=\int_0^1\mu^2e^{-\frac{\kappa_\nu\tau}{\mu}}Q_\nu^+\mathrm{d}\mu-\int_{-1}^0\mu^2e^{-\frac{\kappa_\nu(Z-\tau)}{|\mu|}}Q_\nu^-\mathrm{d}\mu\\
&+\int_0^1\int_0^\tau e^{-\frac{\kappa_\nu(\tau-t)}{\mu}}\kappa_\nu\mathcal{S}_\nu(t)\mathrm{d}t-\int_{-1}^0\int_\tau^Z e^{-\frac{\kappa_\nu(t-\tau)}{|\mu|}}\kappa_\nu\mathcal{S}_\nu(t)\mathrm{d}t\mathrm{d}\mu
\end{aligned}
\tag{27}
$$

$$
\begin{aligned}
&= \int_0^1 \mu^2 \left(e^{-\frac{\kappa_\nu \tau}{\mu}} Q_\nu^+ - e^{-\frac{\kappa_\nu (Z-\tau)}{|\mu|}} Q_\nu^- \right) \mathrm{d}\mu \\
&+ \int_0^\tau \int_0^1 e^{-\frac{\kappa_\nu (\tau - t)}{\mu}} \kappa_\nu (\mathcal{R}_\nu(t) + \mathcal{P}_\nu(t)\mu^2) \mathrm{d}\mu \mathrm{d}t \\
&- \int_\tau^Z \int_0^1 e^{-\frac{\kappa_\nu (t-\tau)}{|\mu|}} \kappa_\nu (\mathcal{R}_\nu(t) + \mathcal{P}_\nu(t)\mu^2) \mathrm{d}\mu \mathrm{d}t \\
&= E_4(\kappa_\nu \tau) Q_\nu^+ - E_4(\kappa_\nu (Z-\tau)) Q^- \\
&+ \int_0^\tau E_2(\kappa_\nu(\tau - t)) \mathcal{R}_\nu(t) \mathrm{d}t - \int_\tau^Z E_2(\kappa_\nu(t-\tau)) \mathcal{R}_\nu(t) \mathrm{d}t \\
&+ \int_0^\tau E_4(\kappa_\nu(\tau - t)) \mathcal{P}_\nu(t) \mathrm{d}t - \int_\tau^Z E_4(\kappa_\nu(t-\tau)) \mathcal{P}_\nu(t) \mathrm{d}t.
\end{aligned}
\tag{28}
$$

□

5.3 Numerical Simulations

At the top of the atmosphere, we are told, the solar radiation intensity is $340W/m^2$ but the atmosphere reflects 30% of it and our RTE does not handle volumic reflection. At 10 or 12km the sunlight is diffused, so we apply an intensity proportional to $\boldsymbol{\omega}_3$. Paris being at latitude 45^0, the radiation is divided by $\sqrt{2}$. Hence an effective number is $Q_{sun} = 162W/m^2$. And yet a good portion is spent for the evaporation of water and into convection. Arbitrarily we keep only half $80W/m^2$.

Recall the scalings defined in [10]. The frequencies and the temperatures are scaled as follows (primes label scaled variables),

$$
\nu' = 10^{-14}\nu, \quad T' = 10^{-14}\frac{k}{h}T = 10^{-14}\frac{1.381 \cdot 10^{-23}}{6.626 \cdot 10^{-34}}T = \frac{T}{4798}.
$$

Planck's function is written as

$$
B_0 \frac{\nu'^3}{e^{\frac{\nu'}{T'}} - 1}, \quad \text{with } B_0 = \frac{2h}{c^2}10^{42} = \frac{2 \times 6.626 \cdot 10^{-34}}{2.998^2 \cdot 10^{16}}10^{42} = 1.4744 \cdot 10^{-8}.
$$

Consequently the computed intensity, I'_ν, is the physical intensity divided by B_0. The scaled Sun temperature is $T'_S = 5800/4798 = 1.209$. According to (18),

$$
\int_0^\infty Q_\nu^+ = 80 = Q^S \int_0^\infty B_0 \frac{\nu'^3}{e^{\frac{\nu'}{T'_S}} - 1} (10^{14} \mathrm{d}\nu') = Q^S 1.4744 \cdot 10^6 \frac{\pi^4}{15} 1.209^4.
$$

This leads to $Q^S = 4 \cdot 10^{-6}$.

Similarly Earth is at $T'_E = 288/4798 = 0.06$ and emits about $350W/m^2$, but some is used for the evaporation of water so we have kept only $300W/m^2$:

$$300 = Q^E \int_0^\infty B_0 \frac{\nu'^3}{e^{\frac{\nu'}{T'_E}} - 1}(10^{14}\mathrm{d}\nu') = Q^E 1.4744 \cdot 10^6 \frac{\pi^4}{15} 0.06^4 = Q^E 124.3.$$

This leads to $Q^E = 2.41$.

The air density is $1 - \frac{3}{4}z$. The earth reflective albedo is set at $r_\nu = 0.3$. Isotropic scattering is set at $a_\nu = 0.3$.

κ_ν is given by the Gemini experimental program. To measure the temperature perturbation due to an increase of $\mathtt{CO}_2$ (resp $\mathtt{NO}_x$)in the atmosphere, we set $\kappa_\nu = 1$ in the range $(3/16, 3/14)$ (resp. $(3/7, 3/5)$.

5.3.1 Isotropic Scattering

Two tests were performed with the stratified 1D approximation, isotropic scattering, no cloud and Gemini κ_ν + Rayleigh scattering equal to 0.3 for $\nu > 3$ and $\tau > 0.7$. One computation is with an infrared source Q^E at $\tau = 0$ only (similar to the situation at night) and another with a sunlight source Q^S at $\tau = Z$ only.

Results are on Figures 3, 4. Computations are done with 3 different atmospheres. One is conform to the Gemini measurements, the other two imitate an addition of $\mathtt{CO}_2$ or methane.

One can observe a small additional greenhouse effect due to addition of $\mathtt{CO}_2$ but a cooling effect at high altitude. The opposite is observed for addition of $\mathtt{NO}_x$.

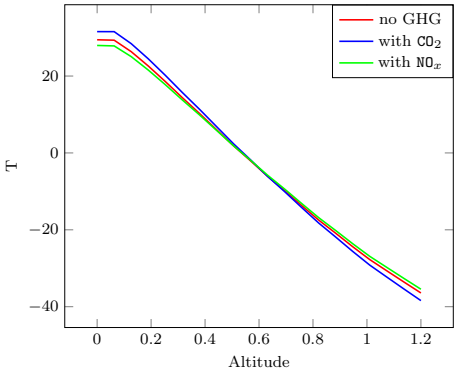

Fig. 3 Temperature T versus altitude z for 3 values of $\nu \mapsto \kappa_\nu$. Only the earth radiation is taken as a source. (night time).

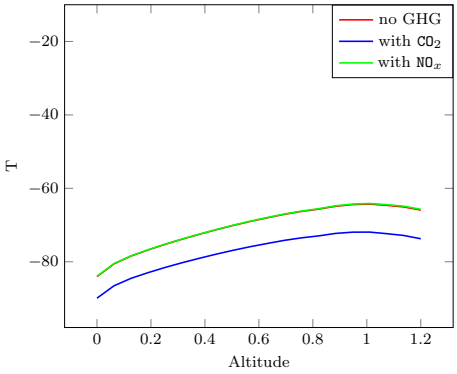

Fig. 4 T vs z for 3 values of $\nu \mapsto \kappa_\nu$. Only the Sun radiation is taken as a source.

5.3.2 Anisotropic Scattering in a Cloud

Next, still with the stratified approximation, a cloud is added between altitude $Z_m = 7000$m and $Z_M = 9000$m with anisotropic scattering coefficient $\beta = \frac{a_\nu}{2}$, $b = 1$, $a_\nu = 0.3\frac{4}{(Z_M - Z_m)^2}(z - Z_m)^+(Z_M - z)^+$. Above Z_M Rayleigh scattering $0.31_{\nu>3}$, replaces the anisotropic scaattering.

Results are shown on Figure 5, 6 and 7. The strong effect of the cloud is shown on Figure 6. Figure 7 shows how important it is to take all the details of κ_ν into account.

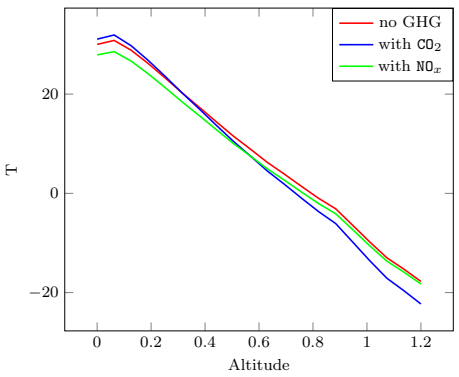

Fig. 5 T versus z computed with a cloud

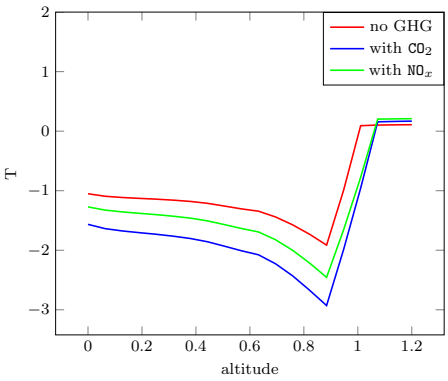

Fig. 6 Difference $T_{nocloud}$ - T_{cloud}

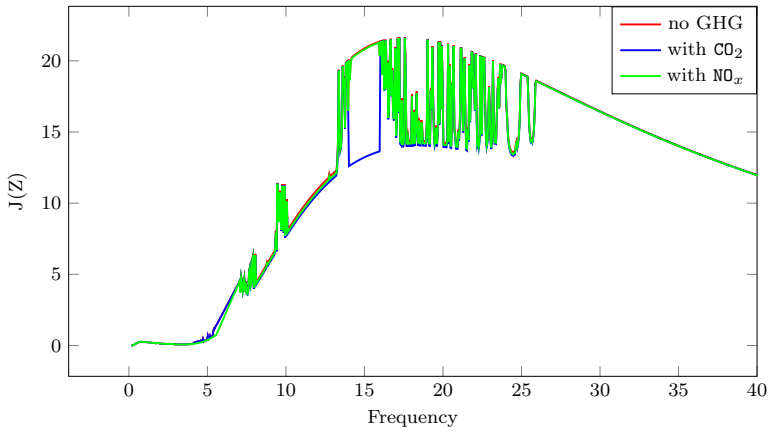

Fig. 7 Radiative intensity $J_\nu(Z)$ versus ν for the 3 $\nu \mapsto \kappa_\nu$ cases.

Finally, in Table 1 total radiative intensities $\int_0^\infty J_\nu(\tau)$ are shown at $\tau = 0$ and $\tau = Z$ in a variety of situations to see the effect of clouds, scattering, earth albedo.

Table 1 Radiative intensities for the Earth radiations + Sunlight (first 2 rows) and the Sunlight only (last 2 rows) when all terms are present and when one of the terms is removed.

	everything	no cloud	no scattering	no earth albedo	no absorption
$\tau = 0$	9.52495	9.39105	9.52441	7.34548	7.21413
$\tau = Z$	5.98738	5.99558	5.98622	4.93935	7.14319
$\tau = 0$	1.44484	1.43589	1.4431	1.51029	1.51029
$\tau = Z$	1.91376	1.90286	1.91093	1.73976	1.51995

In the presence of $\mathtt{CO}_2$ the total radiative energy at ground level (resp. $\tau = Z$), is 9.91316 (resp. 5.72292). With $\mathtt{NO}_x$ it is 9.55564 (resp. 5.8434). These numbers must be compared with the first number on the left in the first (resp 2^{nd}) row in Table 1.

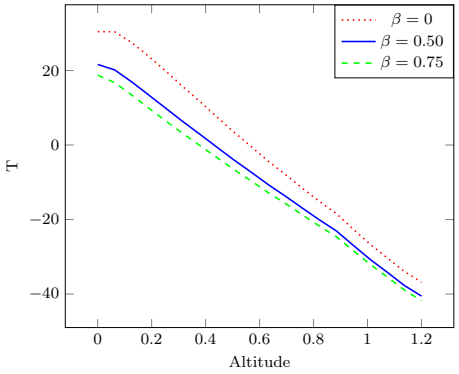

Fig. 8 T versus z computed with a cloud with anisotropic scattering of coefficient β.

6 A 3D formulation with a Stratified Part

To implement in 3D the Earth albedo (reflective condition by the ground) in all generality is quite complicated. To simplify the computation we consider the reflection of the sunlight only and we use the linearity, with respect to the sources, of the equation for I_ν, for a fixed temperature field.

For a portion Ω of atmosphere between the ground $\boldsymbol{g} = (\boldsymbol{x}_1, \boldsymbol{x}_2, \boldsymbol{x}_3 = g(\boldsymbol{x}_1, \boldsymbol{x}_2))$, $g \geq 0$, and the lower stratosphere $\boldsymbol{x}_3 = Z$, consider

$$\begin{aligned} \boldsymbol{\omega} \cdot \boldsymbol{\nabla}_{\boldsymbol{x}} I_\nu + \rho \bar{\kappa}_\nu a_\nu \left[I_\nu - \frac{1}{4\pi} \int_{\mathbb{S}^2} p_\nu(\boldsymbol{\omega}, \boldsymbol{\omega}') I_\nu(\boldsymbol{\omega}') \mathrm{d}\omega' \right] \\ = \rho \bar{\kappa}_\nu (1 - a_\nu)[B_\nu(T) - I_\nu], \\ I_\nu|_{\boldsymbol{g}, \boldsymbol{\omega} \cdot \boldsymbol{n} < 0} = Q^E (\boldsymbol{\omega} \cdot \boldsymbol{n})^- B_\nu(T_E), \quad I_\nu|_{Z, \boldsymbol{\omega}_3 < 0} = Q^S \boldsymbol{\omega}_3^- B_\nu(T_S). \end{aligned} \tag{29}$$

The solution is $I_\nu = I_\nu^E + I_\nu^S$ with I_ν^E computed with the condition $I_\nu|_{\boldsymbol{g}}$ only and the source term in T, and I_ν^S computed with $I_\nu|_Z$ only and $T = 0$:

$$\begin{cases} \boldsymbol{\omega} \cdot \boldsymbol{\nabla}_{\boldsymbol{x}} I_\nu^S + \rho \bar{\kappa}_\nu a_\nu \left[I_\nu^S - \frac{1}{4\pi} \int_{\mathbb{S}^2} p_\nu(\boldsymbol{\omega}, \boldsymbol{\omega}') I_\nu^S(\boldsymbol{\omega}') \mathrm{d}\omega' \right] + \rho \bar{\kappa}_\nu (1 - a_\nu) I_\nu^S = 0, \\ \quad I_\nu^S|_{Z, \boldsymbol{\omega}_3 < 0} = Q^S \boldsymbol{\omega}_3^- B_\nu(T_S), \qquad I_\nu^S|_{0, \boldsymbol{\omega}_3 > 0} = 0, \end{cases}$$

$$\begin{cases} \boldsymbol{\omega} \cdot \boldsymbol{\nabla}_{\boldsymbol{x}} I_\nu^E + \rho \bar{\kappa}_\nu a_\nu \left[I_\nu^E - \frac{1}{4\pi} \int_{\mathbb{S}^2} p_\nu(\boldsymbol{\omega}, \boldsymbol{\omega}') I_\nu^E(\boldsymbol{\omega}') \mathrm{d}\omega' \right] \\ \qquad = \rho \bar{\kappa}_\nu (1 - a_\nu)[B_\nu(T) - I_\nu^E], \\ \quad I_\nu^E|_{g, \boldsymbol{\omega} \cdot \boldsymbol{n} < 0} = Q^E (\boldsymbol{\omega} \cdot \boldsymbol{n})^- B_\nu(T_E) - I_\nu^S|_{\boldsymbol{g}, \boldsymbol{\omega}}, \quad I_\nu^E|_{Z, \boldsymbol{\omega}_3 < 0} = 0. \end{cases} \tag{30}$$

For I_ν^S the stratified approximation is justified. Furthermore, it can be precomputed beforehand.

To account for the fact that a fraction $r_\nu(\boldsymbol{x})$ of the sunlight is reflected by the Earth surface, we consider a partial reflective condition

$$I_\nu^E|_{\boldsymbol{g}, \boldsymbol{\omega} \cdot \boldsymbol{n} < 0} = -I_\nu^S|_{\boldsymbol{g}, \boldsymbol{\omega}} + Q^E (\boldsymbol{\omega} \cdot \boldsymbol{n})^- B_\nu(T_E) + r_\nu(\boldsymbol{g}) I_\nu^S|_{\boldsymbol{g}, \boldsymbol{\omega} - 2(\boldsymbol{\omega} \cdot \boldsymbol{n})\boldsymbol{n}},$$

but $I_\nu^S|_{\boldsymbol{g}, \boldsymbol{\omega}} \approx 0$ when $\boldsymbol{\omega} \cdot \boldsymbol{n} < 0$, so, neglecting scattering, $a_\nu = 0$ (see also [1])

$$I_\nu^S(\boldsymbol{x}, \boldsymbol{\omega}) = \boldsymbol{\omega}_3^- Q^S B_\nu(T_S) \mathrm{e}^{-\kappa_\nu \frac{Z - \tau(\boldsymbol{x}_3)}{\boldsymbol{\omega}_3^-}}.$$

Therefore, with $\boldsymbol{\omega} \cdot \boldsymbol{n} < 0$ and $\boldsymbol{x}$ on the ground,

$$\begin{aligned} -I_\nu^S|_{\boldsymbol{g}, \boldsymbol{\omega}} + r_\nu(\boldsymbol{x}) I_\nu^S|_{\boldsymbol{g}, \boldsymbol{\omega} - 2(\boldsymbol{\omega} \cdot \boldsymbol{n})\boldsymbol{n}} \\ = (\boldsymbol{\omega}_3 - 2(\boldsymbol{\omega} \cdot \boldsymbol{n})\boldsymbol{n}_3)^- Q^S B_\nu(T_S) r_\nu(\boldsymbol{g}) \mathrm{e}^{-\frac{\kappa_\nu (Z - \tau(g))}{(\boldsymbol{\omega}_3 - 2(\boldsymbol{\omega} \cdot \boldsymbol{n})\boldsymbol{n}_3)^-}}. \end{aligned} \tag{31}$$

For a flat ground, it is equal to $\boldsymbol{\omega}_3^+ Q^S B_\nu(T_S) r_\nu(\boldsymbol{g}) \mathrm{e}^{-\frac{\kappa_\nu Z}{\boldsymbol{\omega}_3^+}}$ and its angle average on $\mathbb{S}^2$ is $\frac{1}{2} Q^S B_\nu(T_S) r_\nu(\boldsymbol{g}) E_3(\kappa_\nu Z)$ so that it makes sense to solve the problem with the following conditions,

$$\begin{aligned} I_\nu|_{\boldsymbol{g}, \boldsymbol{\omega} \cdot \boldsymbol{n} < 0} &= (\boldsymbol{\omega} \cdot \boldsymbol{n})^- \left(Q^E B_\nu(T_E) + Q^S B_\nu(T_S) 2 r_\nu(\boldsymbol{g}) E_3(\kappa_\nu Z) \right), \\ I_\nu|_{Z, \boldsymbol{\omega}_3 < 0} &= (\boldsymbol{\omega} \cdot \boldsymbol{n})^- Q^S B_\nu(T_S). \end{aligned} \tag{32}$$

The valley of Chamonix is considered in the same physical conditions as above, i.e. with a cloud between 7000m and 9000m. However we have not implemented the anisotropic scattering yet, so $\beta = 0$.

All 4 vertical boundaries which limit the domain Ω are reflective. Results are shown on Figures 9 and 10.

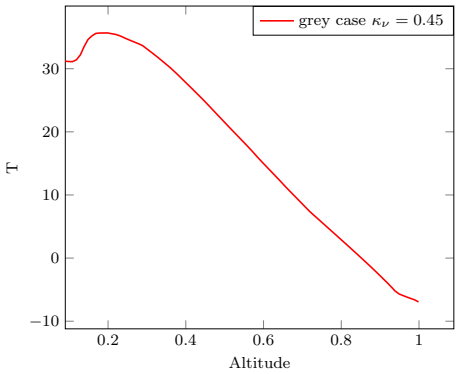

Fig. 9 Temperature above the city of Chamonix versus altitude in a grey case. The growth of T from the ground up is partially due to quadrature errors, partially to the parabolic effect of mountains.

Conclusion

The integro-differential formulation of the RTE and its solution by iterations on the source has been extended here to handle anisotropic scattering.

The iterative part of the method is $O(N \ln N)$, thanks to an efficient use of $\mathcal{H}$-matrices.

The precision is good enough to evaluate the effect of sensitive parameters for the study of contrails. Most of the time the stratified 1D approximation should suffice, but in complex cases with high relief the 3D formulation is needed.

References

1. C. Bardos, F. Golse, and O. Pironneau, Remarks on the Radiative Transfer Equations for Climatology, vol. Impact of Scientific Computing on Science and Society of series Computational Methods in Applied Sciences., Springer Nature, 2023.
2. C. Bardos and O. Pironneau, Radiative transfer for the greenhouse effect, SeMA J. Springer, 79 (2021), pp. 489–525. Special Issue ICIAM 2019.
3. M. Bebendorf, Approximation of boundary element matrices, 86 (2000), pp. 565–589.

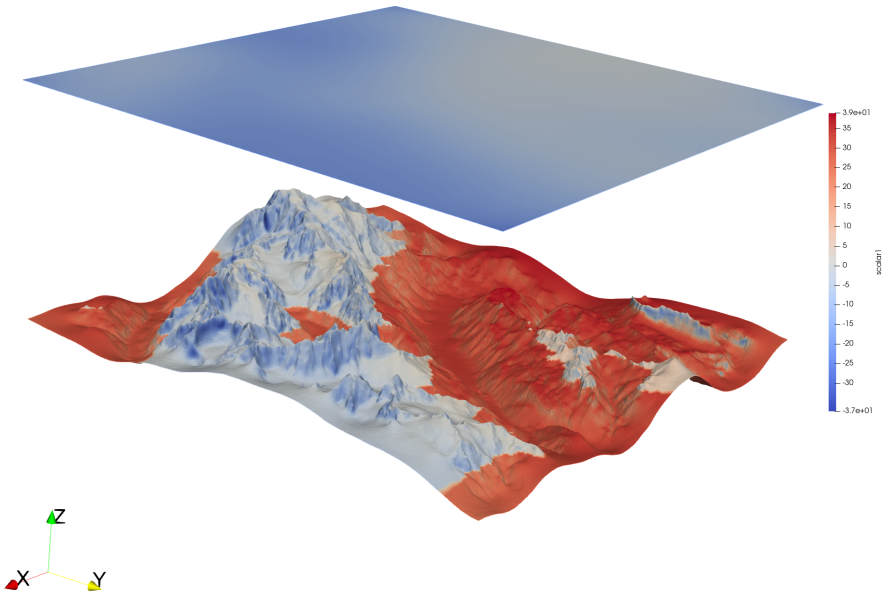

Fig. 10 Ground and high altitude temperature in an atmosphere receiving sunlight and Earth infrared radiation. In addition 0.3% of the sunlight is reflected in the normal direction of the ground and 0.7% if the ground is covered by snow.

4. M. Bebendorf, Hierarchical Matrices, Lecture notes in science and engineering, Springer, Heidelberg, 2008.
5. R. Cahalan, L. Oreopoulos, A. Marshak, K. Evans, A. Davis, and et al., Bringing together the most advanced radiative transfer tools for cloudy atmospheres, American Meteorological Society, 86 (2005), pp. 1275–1294.
6. C. Emde, R. Buras-Schnell, A. Kylling, B. Mayer, J. Gasteiger, U. Hamann, J. Kylling, B. Richter, C. Pause, T. Dowling, , and L. Bugliaro, The libradtran software package for radiative transfer calculations, Geosci. Model Dev, 9 (2016), pp. 1647–1672.
7. F. Golse, F. Hecht, O. Pironneau, D. Smetz, and P.-H. Tournier, Radiative transfer for variable 3d atmospheres, J. Comp. Physics, 475 (2023), pp. 1–19.
8. F. Golse and O. Pironneau, Radiative transfer in a fluid, RACSAM, Springer, Volume dedicated to I. Diaz (2022), pp. https://doi.org/10.1007/s13398–022–01362–x.

9. F. Golse and O. Pironneau, Stratified radiative transfer for multidimensional fluids, Comptes Rendus. Mécanique, 350 (2022), pp. 1–15. DOI : 10.5802/crmeca.136.
10. F. Golse and O. Pironneau, Stratified radiative transfer in a fluid and numerical applications to earth science, SIAM Journal on Numerical Analysis, 60 (2022), pp. 2963–3000, https://doi.org/10.1137/21M1459009, https://doi.org/10.1137/21M1459009, https://arxiv.org/abs/https://doi.org/10.1137/21M1459009.
11. W. Hackbusch, A sparse matrix arithmetic based on h-matrices. part i: Introduction to h-matrices, Computing, 62 (1999), pp. 89–108.
12. D. S. Lee, D. W. Fahey, A. Skowron, M. R. Allen, U. Burkhardt, and Q. Chen, The contribution of global aviation to anthropo- genic climate forcing for 2000 to 2018., Atmospheric Environment, 244 (2021), p. 117834.
13. S. Marquart, M. Ponater, F. Mager, and R. Sausen, Future development of contrail cover, optical depth, and radiative forcing: impacts of increasing air traffic and climate change, J. Climate, 16 (2003), pp. 2890–2904.
14. R. Paoli and K. Shariff, Contrail modeling and simulation, Annual Rev. Fluid Mech, 48 (2016), pp. 393–427.
15. O. Pironneau and P.-H. Tournier, Reflective conditions for radiative transfer in integral form with h-matrices. submitted to JCP 2023.
16. G. Pomraning, The equations of Radiation Hydrodynamics, Pergamon Press, NY, 1973.
17. M. Porzio and O. Lopez-Pouso, Application of accretive operators theory to evolutive combined conduction, convection and radiation, Rev. Mat. Iberoamericana, 20 (2004), pp. 257–275.